SUPPORTING INFORMATION

MOF-templated syntheses of porous Co_3O_4 hollow-spheres and micro-flowers for enhanced performance in supercapacitors**

Ziyi Zhu,[a†] Cheng Han,[a†] Ting-Ting Li,[c] Yue Hu,*[a] Jinjie Qian,*[a] and Shaoming Huang[a]

[a]*College of Chemistry and Materials Engineering, Wenzhou University, Wenzhou 325035, P. R. China.*

[b]*School of Materials and Energy, Guangdong University of Technology, Guangzhou, Guangdong 510006, P. R. China.*

[c]*Research Center of Applied Solid State Chemistry, Ningbo University, Ningbo, 315211, P. R. China.*

[†]*These authors contributed equally to this work.*

**To whom correspondence should be addressed: E-mail: jinjieqian@wzu.edu.cn; yuehu@wzu.edu.cn; Tel: 86-577-88373064.*

Table of Content

S1. Materials and Methods S1-S3

S2. TGA Data S4

S3. PXRD Patterns S5

S4. N_2 Isotherms, BET and Langmuir Analyses S6-S15

S5. Additional images for Co-BTB-I/Co-BTB-II Microparticles S16-S19

S6. Electrochemical Measurements S20-S21

S1. Materials and Methods

1.1. Materials and Instruments.

Reactions were carried out in 35 ml pressure-resistant tubes under autogenous pressure. All the reactants are of reagent-grade quality and used as commercially purchased without further purification.

The power X-ray diffraction patterns (PXRD) were collected by a Bruker D8 Advance using Cu Kα radiation (λ = 0.154 nm).

Single gas adsorption measurements were performed in the Accelerated Surface Area and Porosimetry 2020 (ASAP2020, where the bulk **Co-BTB-I/II-450** materials were determined in a clean ultra high vacuum system and the N_2 sorption measurement was performed at 77 K.

Thermogravimetric analyses were recorded on a NETZSCH STA 449C unit at a heating rate of 10 $^{o}C\cdot min^{-1}$ under flowing nitrogen atmosphere.

Field-emission scanning electron microscopy (FE-SEM) images were obtained on a Nova NanoSEM200 scanning electron microscope.

For transmission electron microscopy (TEM), high-resolution transmission electron microscopy (HRTEM), energy dispersive spectroscopy (EDS), high-angle annular dark-field (HAADF), and scanning transmission electron microscopy EDS (STEM-EDS) characterizations, the purified colloid was deposited on copper grids with thin carbon film, which was then dried for 20 min under an infrared lamp. After water was removed completely, the dried sample was observed with a 200 kV JEOL 2100F with an attached EDS and STEM detector.

X-ray photoelectron spectroscopy (XPS) measurements were carried out with a Thermo ESCALAB 250 X-ray photoelectron spectrometer with an excitation source of Al Ka radiation (λ = 1253.6 eV). The binding energies were referenced to the C 1s line at 284.6 eV from adventitious carbon.

1.2. Synthesis of hollow spherical Co-BTB-I.

A mixture of $Co(NO_3)_3 \cdot 6H_2O$ (0.10 mmol, 29.1 mg) and H_3BTB (0.025mmol, 11 mg, H_3BTB = 1,3,5-tris(4-carboyphenyl)benzene) in *N*-methylformamide (NMF) (5 mL) with the surfactant CTAB (0.08 mmol, 30.0 mg, CATB = hexadecyl trimethyl ammonium bromide) as well as an additional 0.05 ml HNO_3 (65 wt %) was placed in a 35 mL pressure-resistant tube, which was inserted into a preheated module holding at 140 ^oC for 45 min, and then gradually cooled to room-temperature. After being centrifugated and washed by fresh ethanol for 3 times, the light pink products of CATB-assisted hollow **Co-BTB-I** micro-spheres were obtained in *ca*. 35% yield based on the organic ligand. The crystalline nature of the sample was confirmed by the powder X-ray diffraction (Figure S2).

1.3. Synthesis of flower-like Co-BTB-II.

Very similarly to the synthesis of **Co-BTB-I**, a mixture of $Co(NO_3)_3 \cdot 6H_2O$ (0.17 mmol, 50 mg) and H_3BTB (0.025mmol, 11 mg) in *N*-dimethylformamide (NMF) (5 mL, without the surfactant CTAB), but still with an additional 0.05 ml HNO_3 (65 wt %) was placed in a 35 mL pressure-resistant tube, which was inserted into a preheated module holding at 140 ^oC for 45 min, and then gradually cooled to room-temperature. After being centrifugated and washed by fresh ethanol, the light pink products of **Co-BTB-II** micro-flowers were obtained in *ca*. 42% yield based on the organic ligand. The crystalline nature of the sample was confirmed by the powder X-ray diffraction (Figure S2).

1.4. Syntheses of Co-BTB-I-450 and Co-BTB-II-450.

Finally, we learn both MOF-based materials retain their crystalline structure before and after desolvation. And spherical Co_3O_4-based micro-particles (**Co-BTB-I-450**) were then synthesized by the direct pyrolysis of **Co-BTB-I** samples at 450 °C in the air in a conventional CVD furnace. During the calcination process, MOF precursors were gradually decomposed to hollow Co_3O_4 particles. Same procedure can be found in the synthesis of **Co-BTB-II-450**, and the compositional phases of

these two kinds of micro-particles have been confirmed by PXRD test (Figure 3, in the main article)

1.4. Electrochemical method.

The electrochemical measurements were carried out in a three-electrode electrochemical cell containing 3.0 M KOH aqueous solution as the electrolyte. Our **Co-BTB-I-450** and **Co-BTB-II-450** samples are uniformly painted onto the surface of pre-treated Ni foam to constitute the **Co-BTB-I/II-450** foam, which were directly used as working electrodes. The area of the working electrodes immersed into the electrolyte was controlled to be ~1 cm^2. The electrochemical measurements were conducted with a CHI760E electrochemical workstation. A saturated Hg/HgO electrode was used as the reference electrode and a platinum wire as the counter electrode, and all the experiments were done at ambient temperature. EIS measurements were performed by applying an AC voltage with 5 mV amplitude in a frequency range from 0.01 Hz to 100 kHz. The mass loading of the active materials on Ni foam were 2~4 mg cm^{-2}

S2. TGA Data

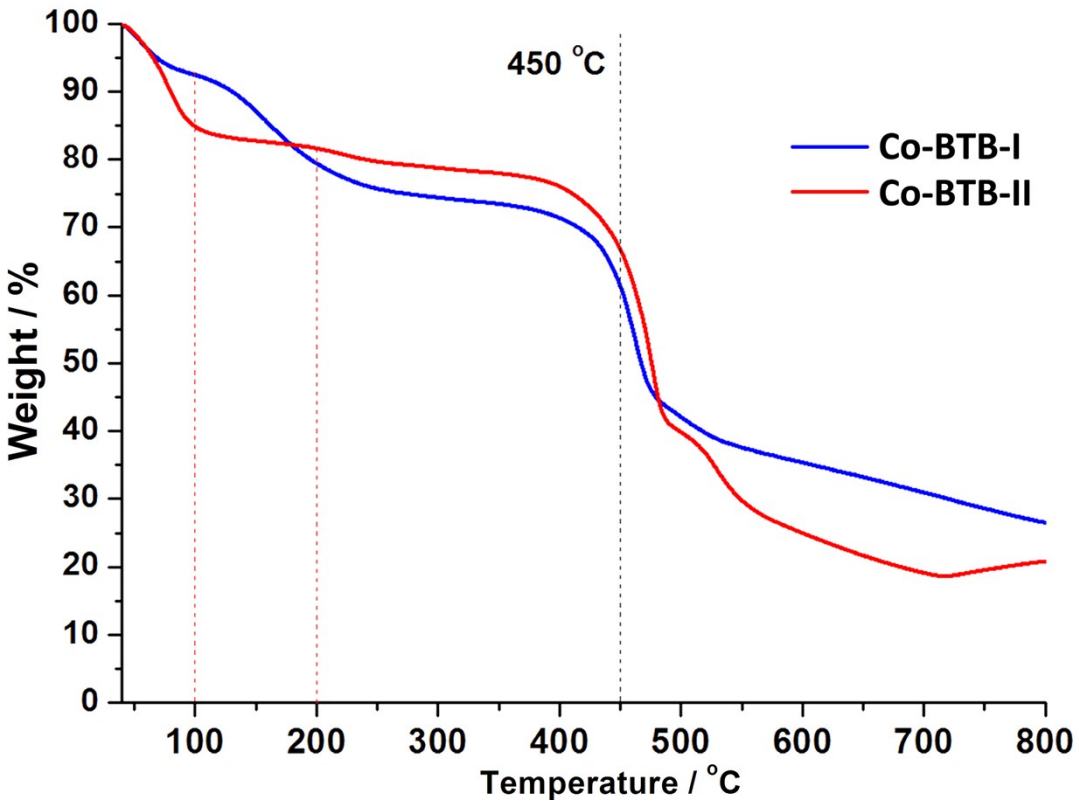

Figure S1. TGA curves for these two as-prepared spherical **Co-BTB-I** and flower-like **Co-BTB-II** samples.

The thermogravimetric analysis (TGA) curve of the as-obtained **Co-BTB-I** as well as **Co-BTB-II** samples are conducted in the temperature range of 30-800 °C under a flow of nitrogen with the heating rate of 10 °C min^{-1}, and they exhibit the first weight loss of 7.5 and 15.1 wt % at the temperature of 100 °C and show another weight loss of ~13.1 and ~3.2 wt% between 100 °C and 200 °C, corresponding to the loss of H_2O molecules and guest N-methylformamide molecule. After **450 °C**, we also learn that the main structure starts to collapse gradually, in which both Co-BTB frameworks begin the breakdown of Co-COO bonds and decomposition of BTB linkers, thus leading to the formation of our targeted Co_3O_4.

S3. PXRD Patterns

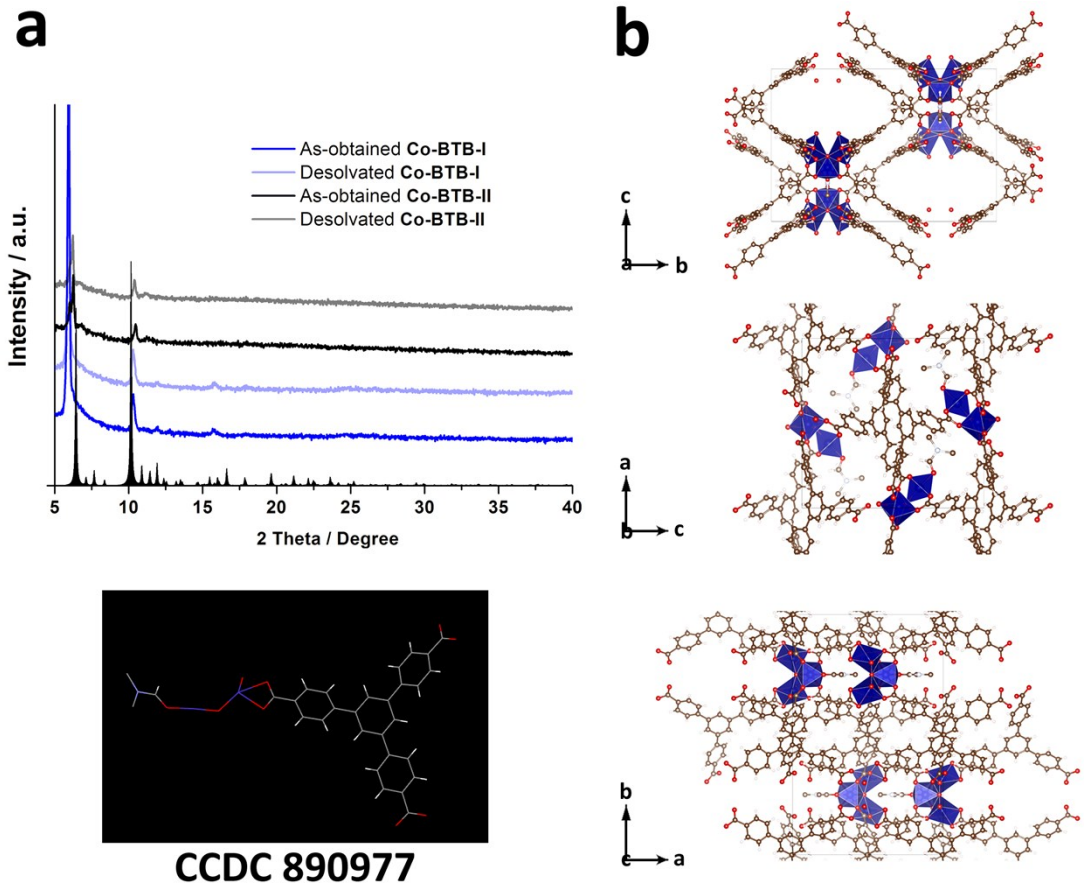

Figure S2. PXRD patterns of spherical **Co-BTB-I** and flower-like **Co-BTB-II**, where two strong peaks centered at 6.0 and 10.4 can be observed which indicate highly ordered and crystalline structures with several other weak peaks.

In order to find the matched structure from the powder X-ray diffraction (PXRD) measurement, we learnt that hollow-Co-BTB (**Co-BTB-I**) and flower-like-Co-BTB (**Co-BTB-II**) micro-particles are crystalline materials (Figure S2a). On the other hand, a similar XRD pattern derived from a Co-BTB MOF structure (from any of the numerous MOF libraries in CCDC database, which is constructed from Co(II) and H_3BTB, CCDC No.: 890977) could be observed as above, while the **VESTA** structures of the **Co-BTB-I** as well as **Co-BTB-II** microparticles viewed from *a, b, c*-axes are presented in the right column.

S4. N_2 Isotherms, BET and Langmuir Analyses

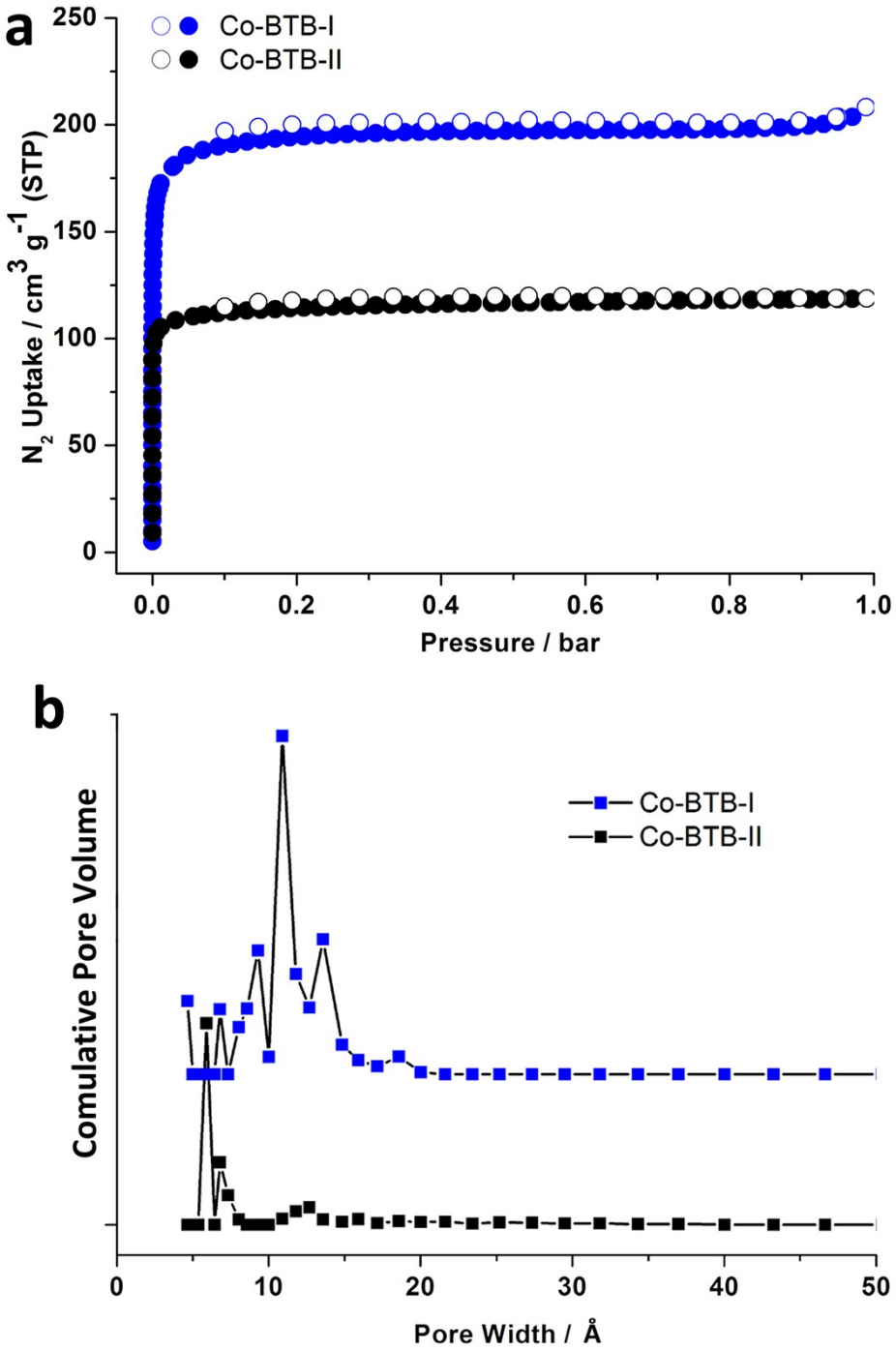

Figure S3. (a) The experimental N_2 adsorption/desorption isotherms at 77 K for the desolvated spherical **Co-BTB-I** and flower-like **Co-BTB-II** samples, both exhibiting the type-I isotherms (typical characteristics of microporous materials); (b) The pore size distribution of these two materials.

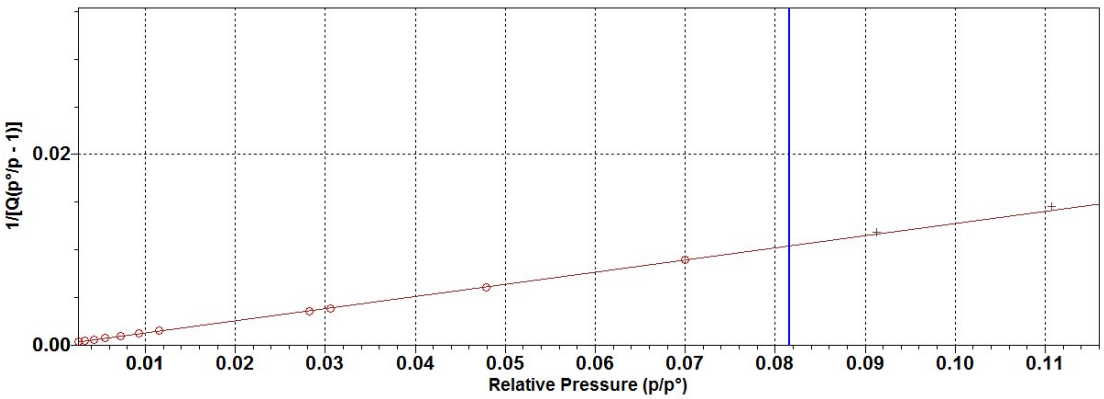

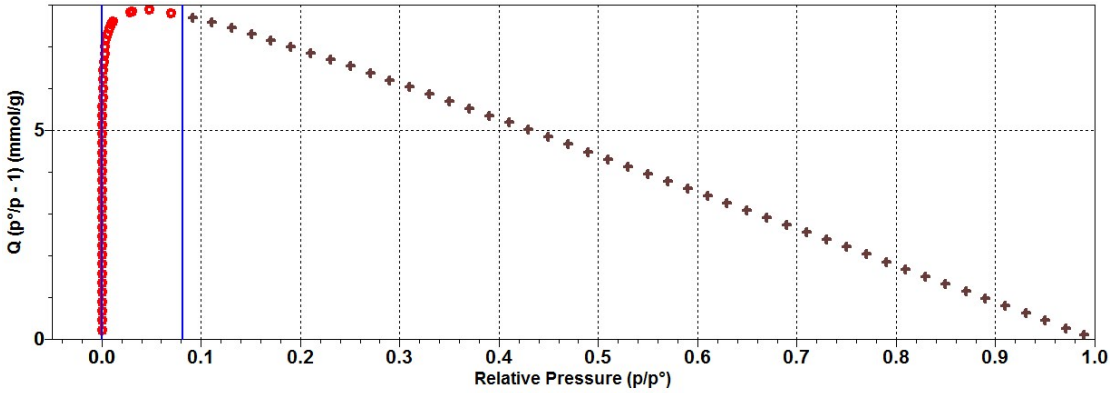

Summary (**Co-BTB-I**)

BET Surface Area: 765.5022 ± 1.3102 m²/g

Slope: 0.127442 ± 0.000218 g/mmol

Y-Intercept: 0.000021 ± 0.000003 g/mmol

C: 6127.834066

Qm: 7.84543 mmol/g

Correlation Coefficient: 0.9999429

Molecular Cross-Sectional Area: 0.1620 nm²

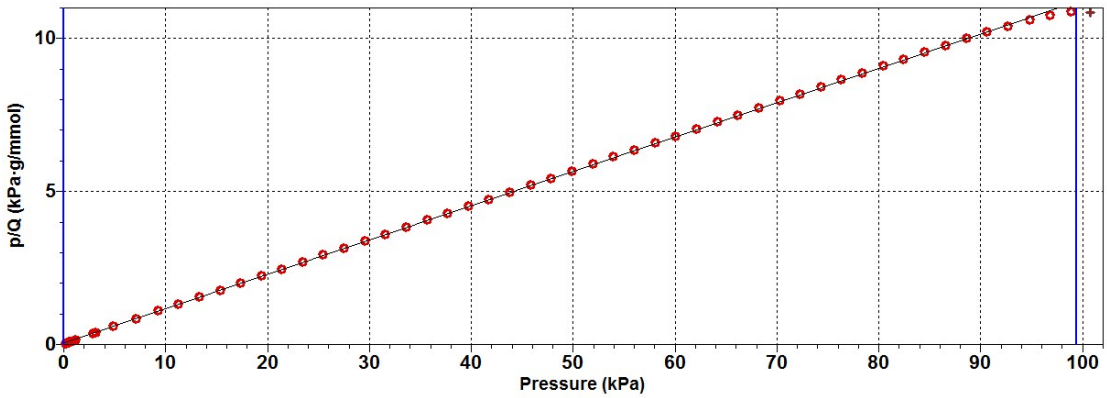

Summary (**Co-BTB-I**)

Langmuir Surface Area: 869.8358 ± 1.5418 m²/g

Slope: 0.11217 ± 0.00020 g/mmol

Y-Intercept: 0.050 ± 0.011 kPa·g/mmol

b: 2.22490 1/kPa

Qm: 8.91471 mmol/g

Correlation Coefficient: 0.999912

Molecular Cross-Sectional Area: 0.1620 nm²

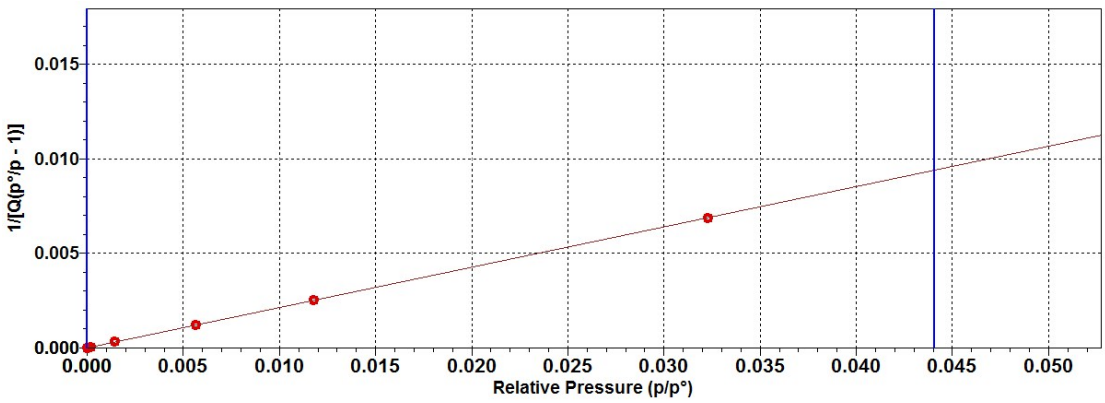

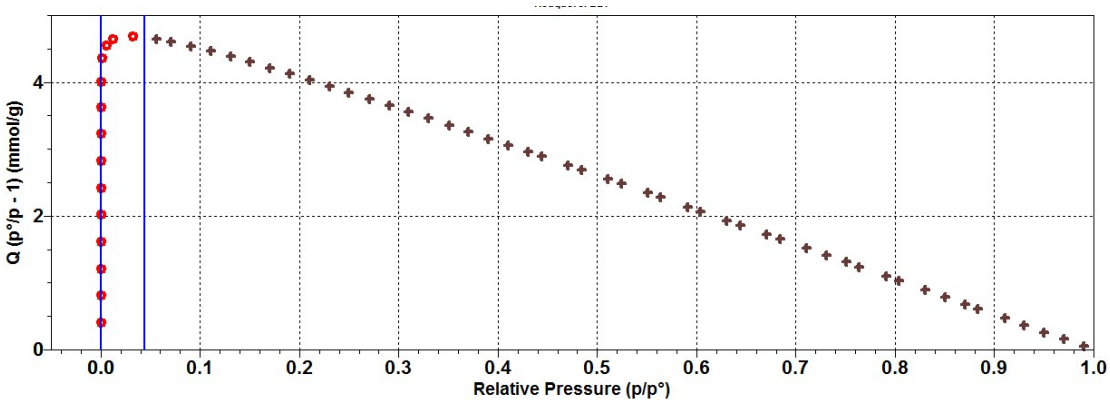

Summary (**Co-BTB-II**)

BET Surface Area: 457.2234 ± 0.7975 m²/g

Slope: 0.213397 ± 0.000372 g/mmol

Y-Intercept: 0.000006 ± 0.000003 g/mmol

C: 33806.297386

Qm: 4.68596 mmol/g

Correlation Coefficient: 0.9999817

Molecular Cross-Sectional Area: 0.1620 nm²

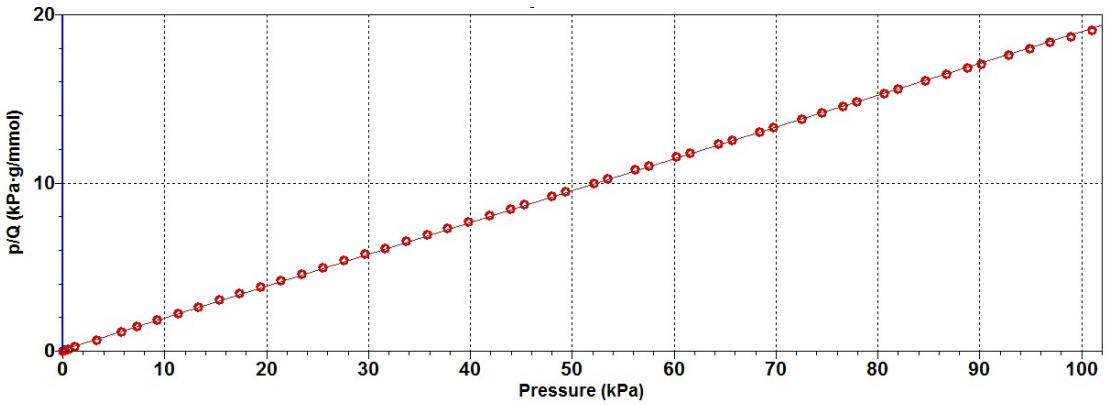

Summary (**Co-BTB-II**)

Langmuir Surface Area: 515.6475 ± 0.6350 m²/g

Slope: 0.18922 ± 0.00023 g/mmol

Y-Intercept: 0.079 ± 0.012 kPa·g/mmol

b: 2.39804 1/kPa

Qm: 5.28473 mmol/g

Correlation Coefficient: 0.999955

Molecular Cross-Sectional Area: 0.1620 nm²

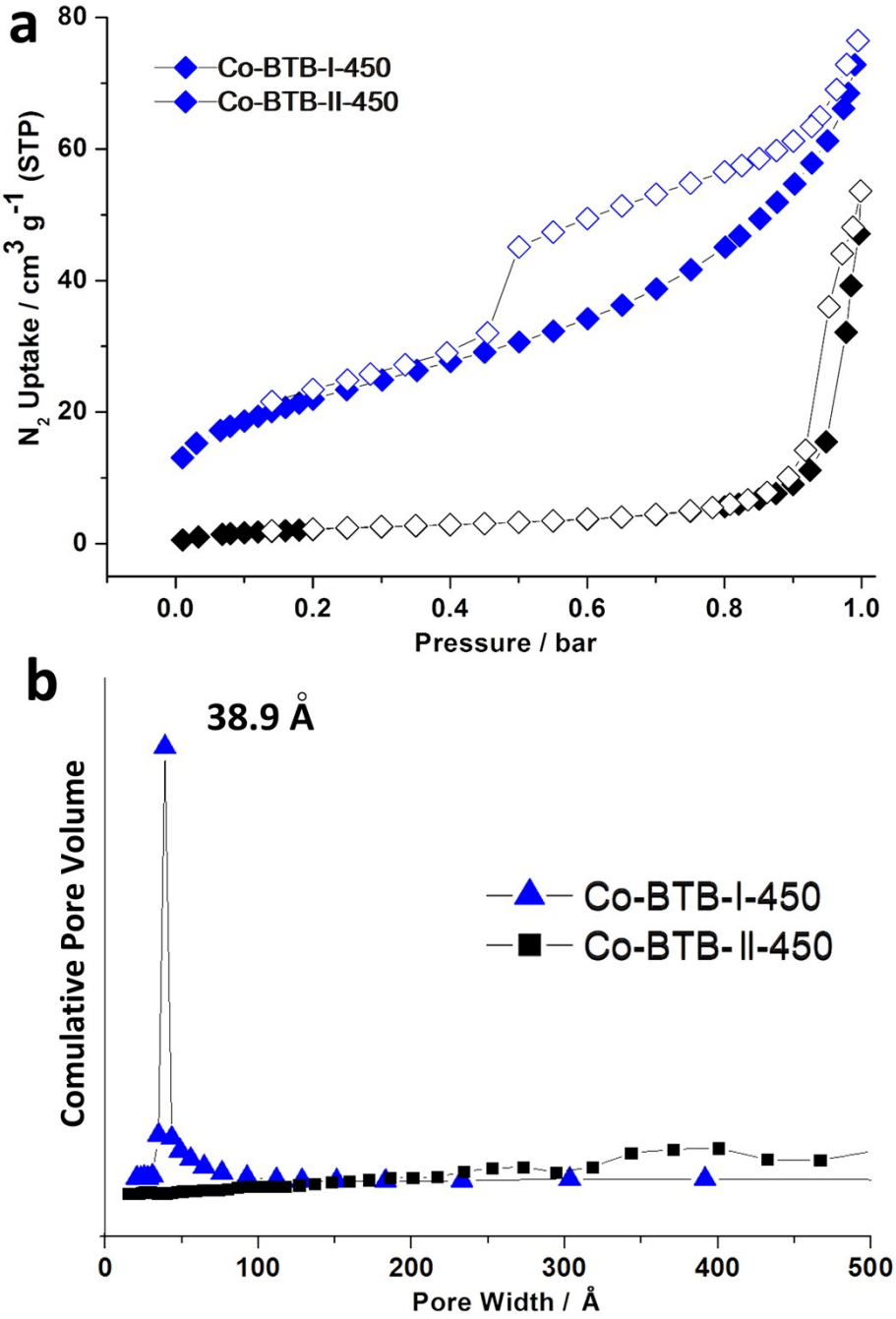

Figure S4. (a) The experimental N_2 adsorption/desorption isotherms at 77 K for the desolvated **Co-BTB-I-450** micro-spheres and **Co-BTB-II-450** micro-flowers, where **Co-BTB-I-450** exhibits the type-IV isotherm with hysteresis loop (typical characteristics of mesoporous materials), while **Co-BTB-II-450** shows the type-III isotherm implying only surface-based adsorption in relatively high pressure zone; (b) Pore size distribution of the desolvated **Co-BTB-I-450** micro-spheres.

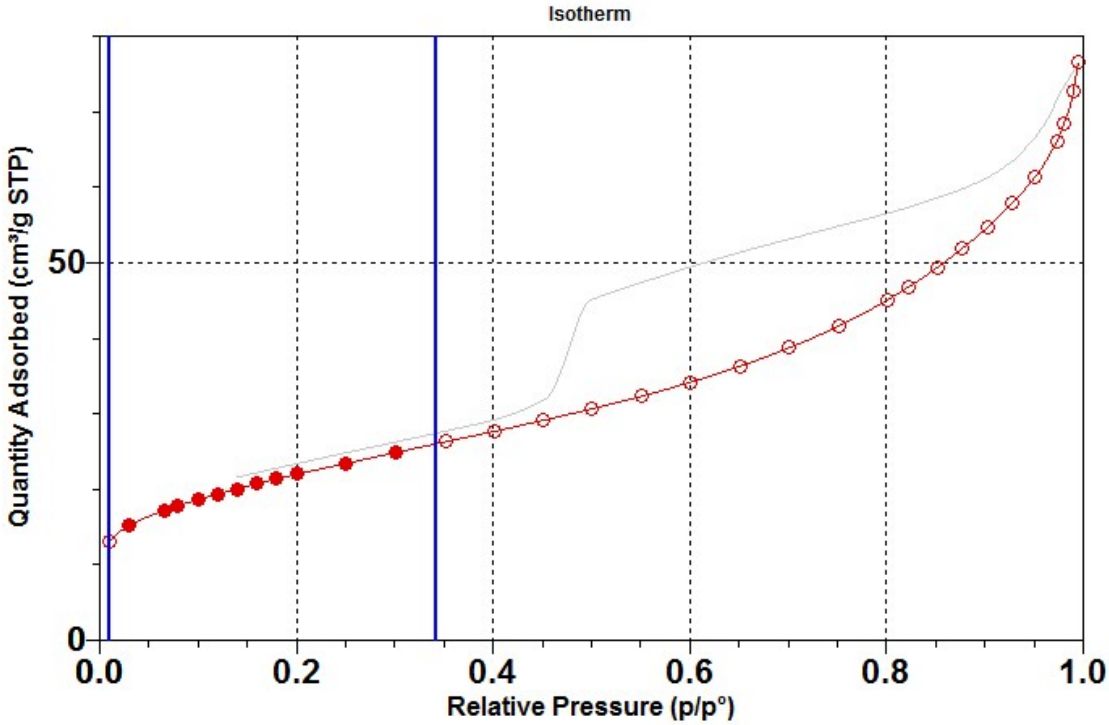
Isotherm
Quantity Adsorbed (cm³/g STP)
50
0
0.0
0.2
0.4
0.6
0.8
1.0
Relative Pressure (p/p°)

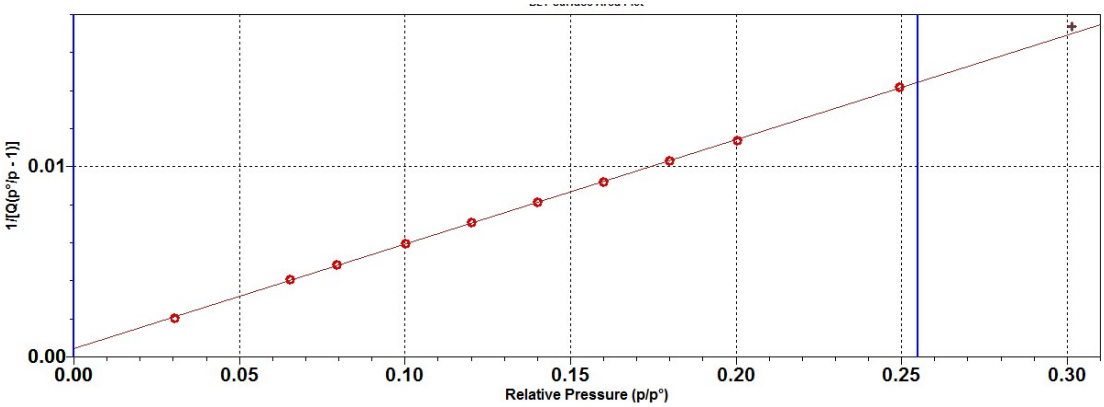
1/[Q(p°/p - 1)]
0.01
0.00
0.00
0.05
0.10
0.15
0.20
0.25
0.30
Relative Pressure (p/p°)

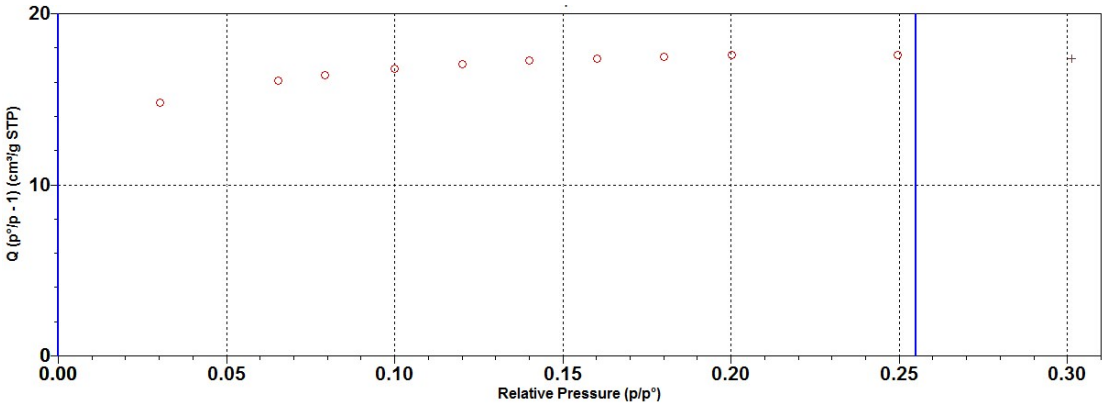
Q (p°/p - 1) (cm³/g STP)
20
10
0
0.00
0.05
0.10
0.15
0.20
0.25
0.30
Relative Pressure (p/p°)

Summary (**Co-BTB-I-450**)

BET Surface Area: 78.6139 ± 0.3196 m^2/g

Slope: 0.054937 ± 0.000223 g/cm^3 STP

Y-Intercept: 0.000438 ± 0.000033 g/cm^3 STP

C: 126.456554

Qm: 18.0589 cm^3/g STP

Correlation Coefficient: 0.9999342

Molecular Cross-Sectional Area: 0.1620 nm^2

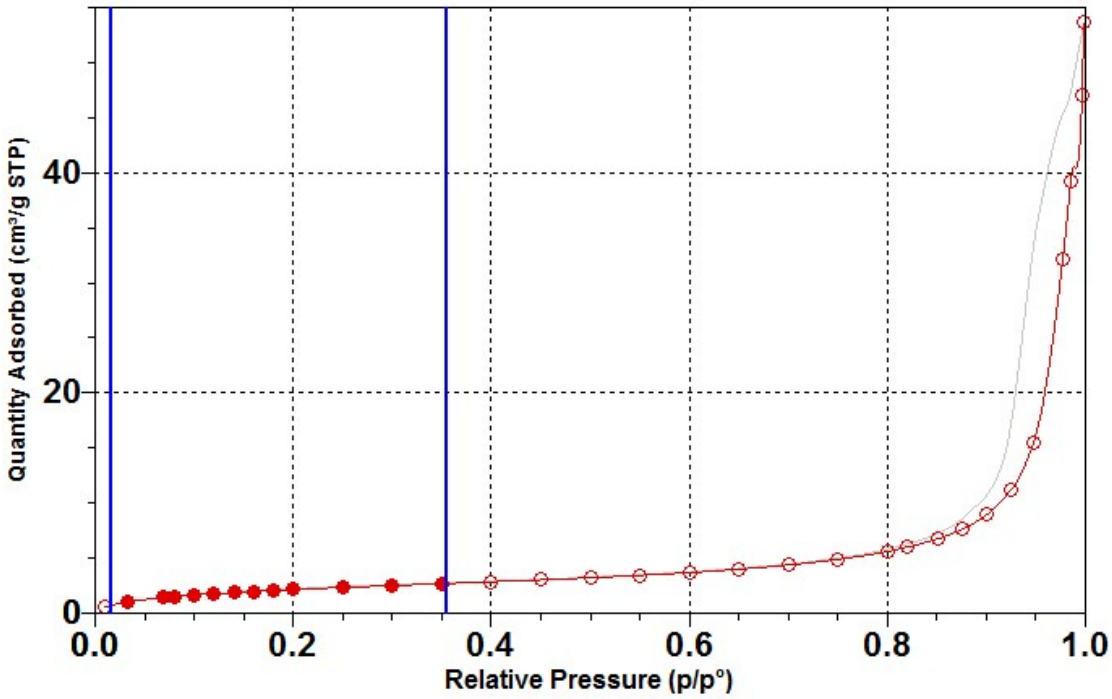
Quantity Adsorbed (cm³/g STP)
0
20
40
0.0
0.2
0.4
0.6
0.8
1.0
Relative Pressure (p/p°)

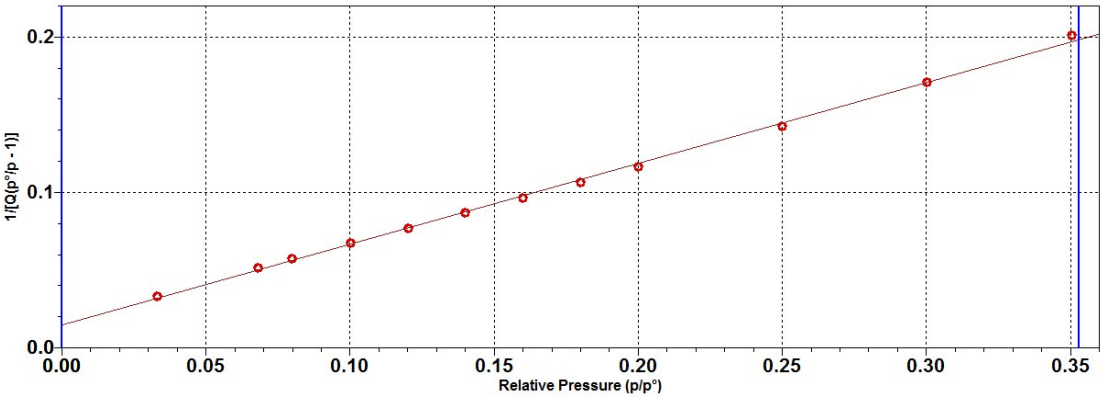
1/[Q(p°/p - 1)]
0.0
0.1
0.2
0.00
0.05
0.10
0.15
0.20
0.25
0.30
0.35
Relative Pressure (p/p°)

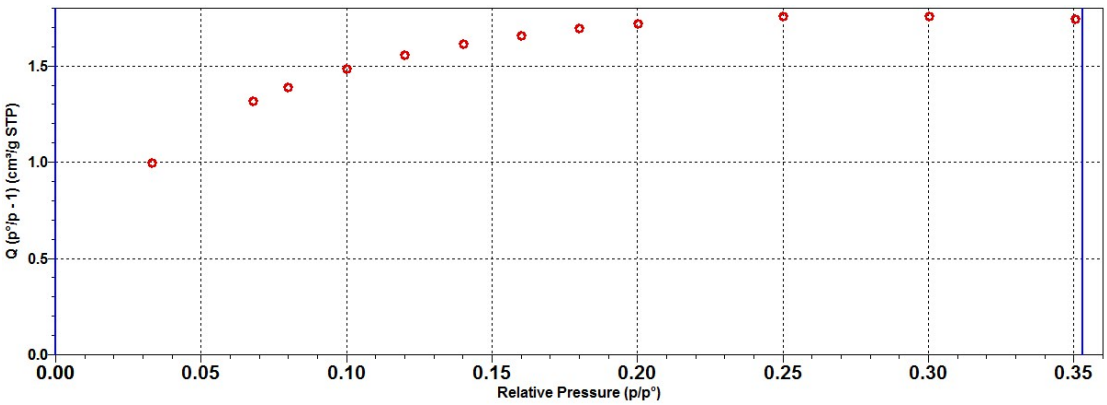
Q (p°/p - 1) (cm³/g STP)
0.0
0.5
1.0
1.5
0.00
0.05
0.10
0.15
0.20
0.25
0.30
0.35
Relative Pressure (p/p°)

Summary (**Co-BTB-II-450**)

BET Surface Area: 8.3141 ± 0.0886 m^2/g

Slope: 0.507433 ± 0.005493 g/cm^3 STP

Y-Intercept: 0.016159 ± 0.000961 g/cm^3 STP

C: 32.402046

Qm: 1.9099 cm^3/g STP

Correlation Coefficient: 0.9995315

Molecular Cross-Sectional Area: 0.1620 nm^2

S5. Additional images for Co-BTB-I/Co-BTB-II Microparticles

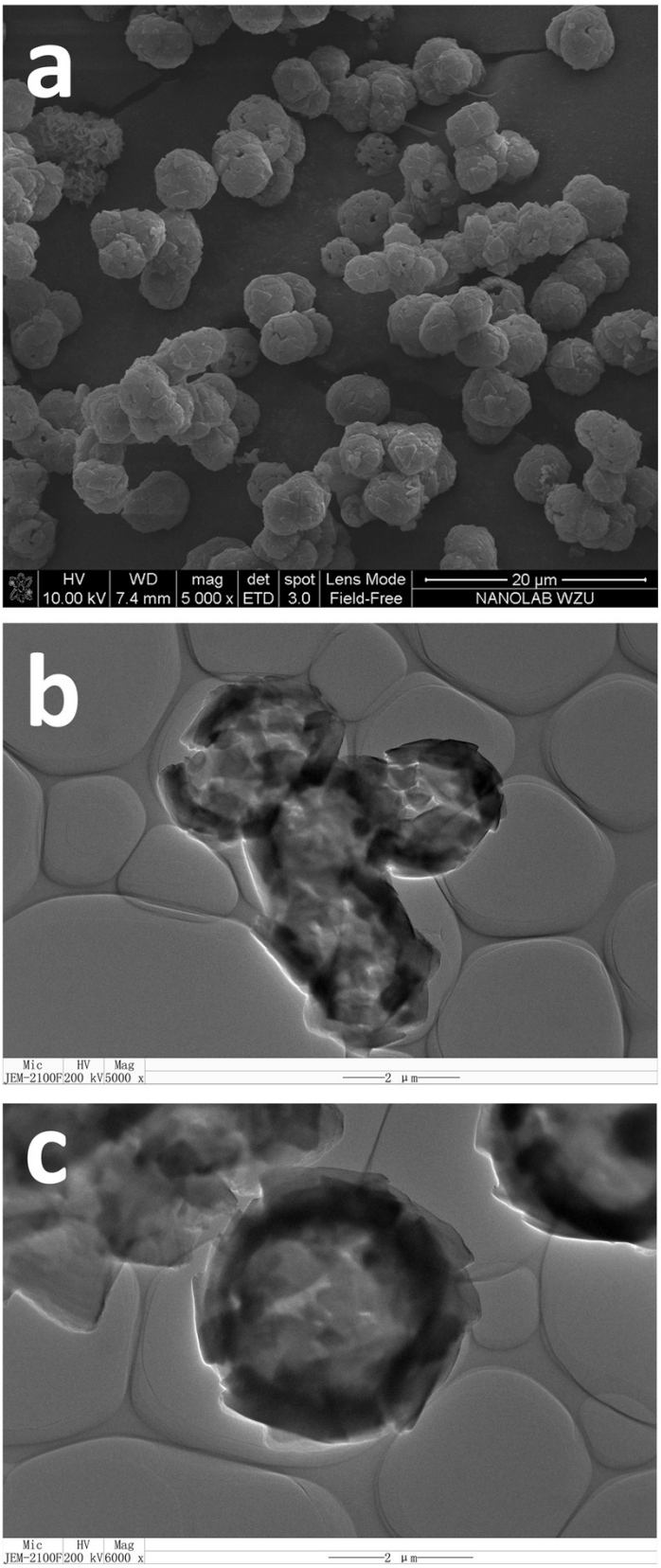

Figure S5. SEM and TEM images of the as-prepared **Co-BTB-I** microspheres.

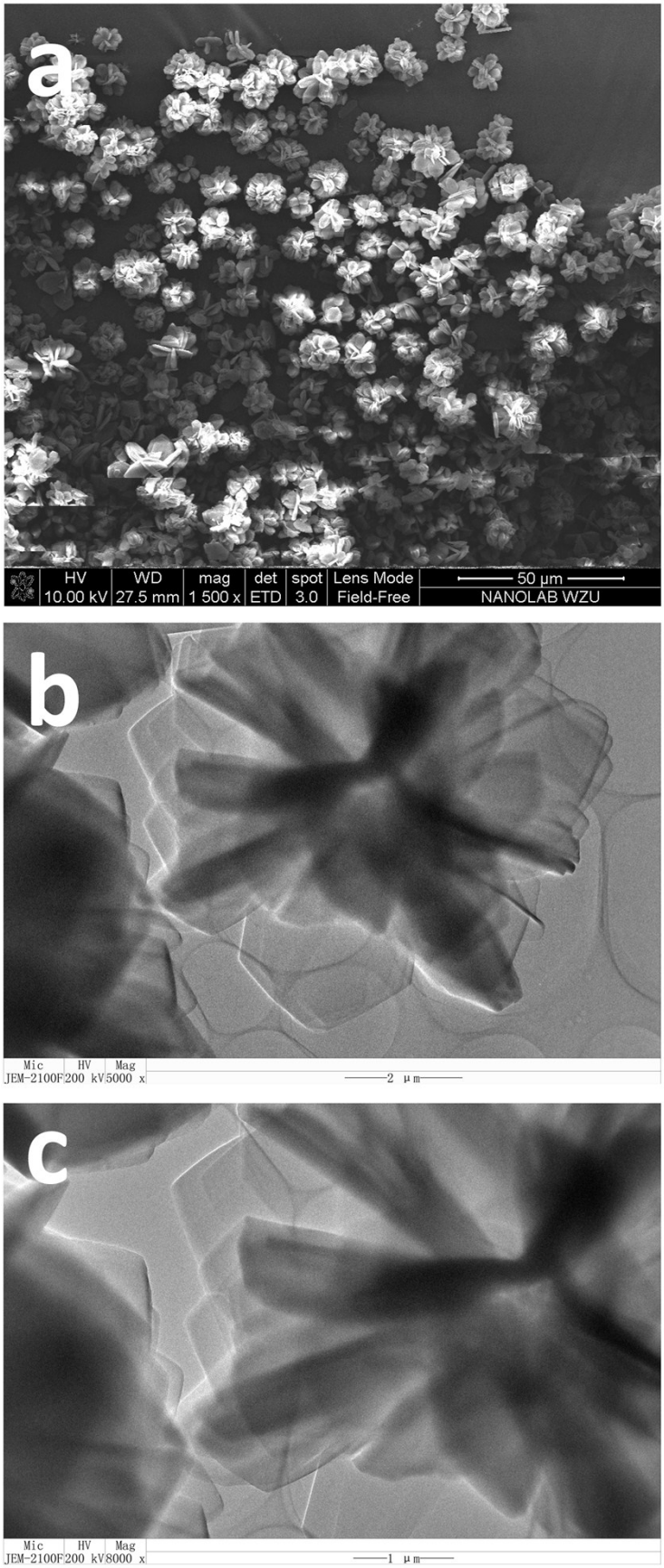

Figure S6. SEM and TEM images of the as-prepared **Co-BTB-II** microflowers.

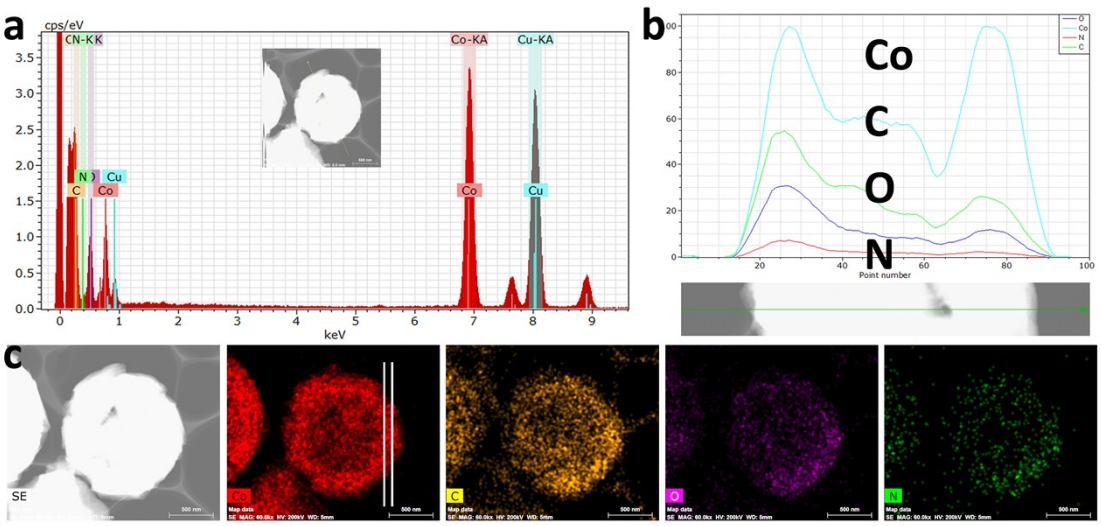

Figure S7. (a) EDX curve of **Co-BTB-I**; (b) Height profiles of single **Co-BTB-I** particle for C N O Co elements; (c) HAADF-STEM images and mapping of **Co-BTB-I** precursors.

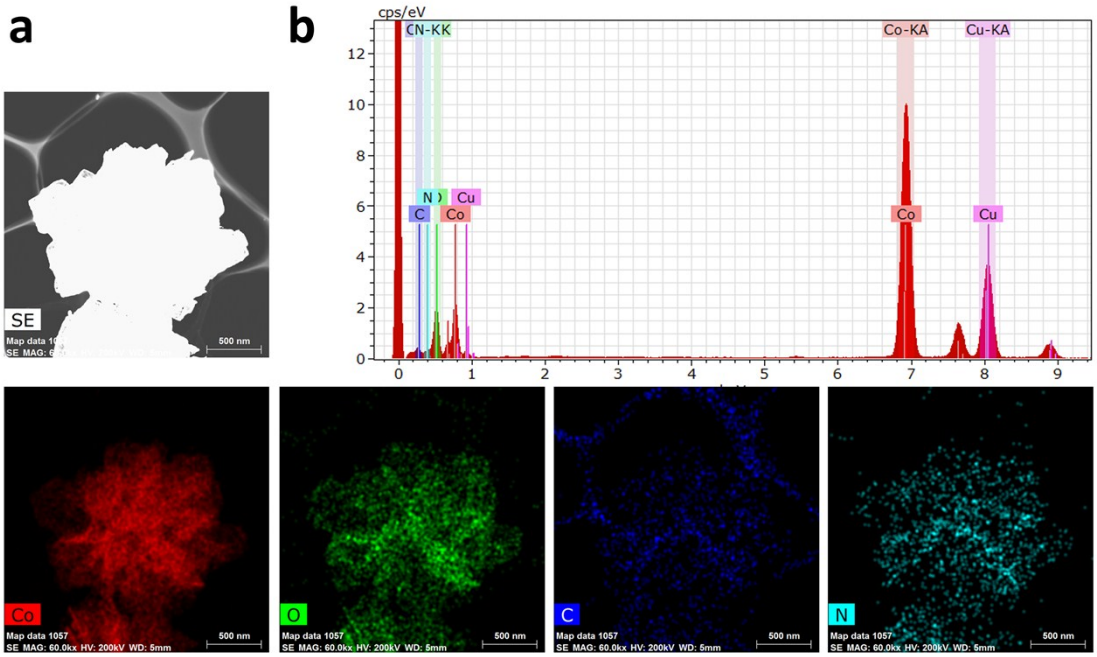

Figure S8. (a) EDX curve of **Co-BTB-II**; (b) Height profiles of single **Co-BTB-II** particle for C N O Co elements; (c) HAADF-STEM images and mapping of **Co-BTB-II** precursors.

S6. Electrochemical Measurements

Two main redox reactions involved in our system could be listed as below:

$$\mathbf{Co_3O_4 + OH^- + H_2O \rightarrow 3CoOOH + e^-}$$

$$\mathbf{CoOOH + OH^- \rightarrow CoO_2 + H_2O + e^-}$$

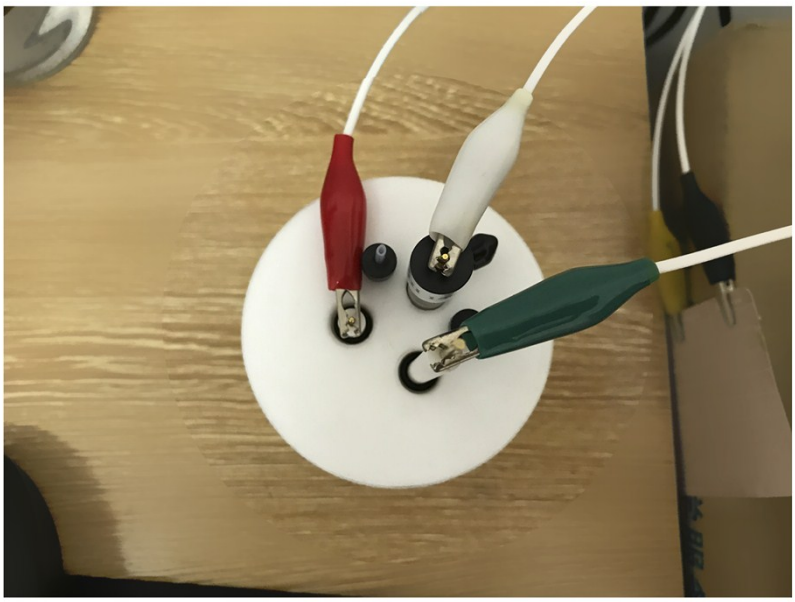

Figure S9. The 3-electrode system we used in our lab.

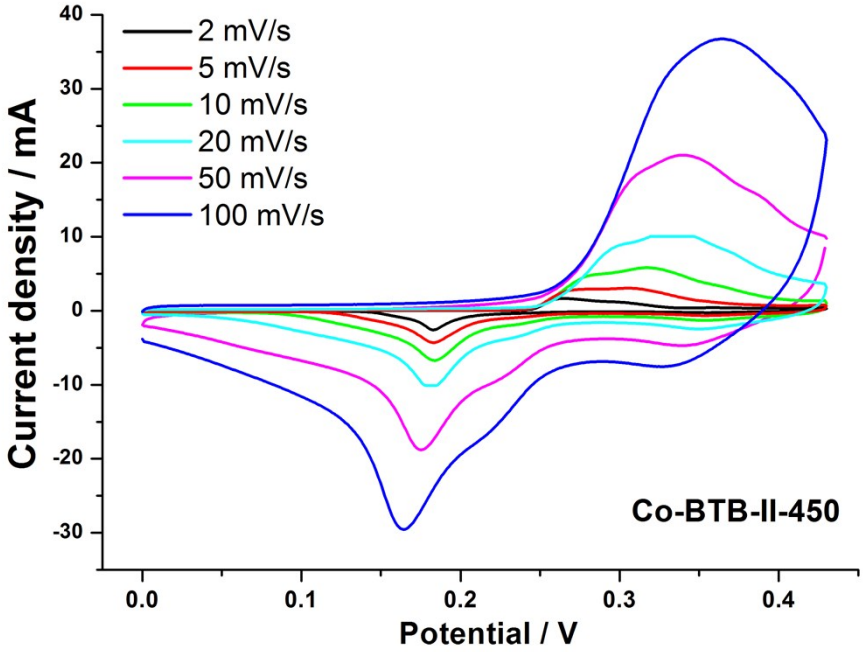

Figure S10. Cyclic voltammograms of **Co-BTB-II-450** at different scan rates of 2-100 mV/s;

For Figure S9 above and for **Figure 4a** in the manuscript, we simultaneously learn that the cathodic potential becomes more negative and the anodic one tends to be more positive in CV curves.

Table 1. The specific capacitance of other reported Co_3O_4 electrode materials:

Catalyst	Substrate	Elecrolyte	Current density	Special capacitance	Ref.
ZnO@Co3O4	Ni foam	2 M KOH	1 A g^{-1}	857.7 F g^{-1}	1
atomic layer Co_3O_4 nanofilm	Ni foam	2 M KOH	1 A g^{-1}	1400 F g^{-1}	2
Co_3O_4/VAGN/CF	carbon fabric	2 M KOH	1 A g^{-1}	3480 F g^{-1}	3
NPC Co_3O_4	GCE	0.1 M KOH	2.5 A g^{-1}	885 F g^{-1}	4
Co_3O_4/GF film	Ni foam	2 M KOH	2 A g^{-1}	652 F g^{-1}	5
Co_3O_4/C NAs	Ni foam	3 M KOH	1 mA cm^{-2}	776.5 F g^{-1}	6
CWs-Co_3O_4	stainless-steel wire mesh	6 M KOH	0.5 A g^{-1}	978.9 F g^{-1}	7
Co_3O_4/CNN	GCE	0.1 M KOH	20 mV s^{-1}	90.8 F g^{-1}	8
Co_3O_4/rGO/NF	Ni foam	1 M KOH	1 A g^{-1}	1016.4 F g^{-1}	9

1. D. Cai, H. Huang, D. Wang, B. Liu, L. Wang, Y. Liu, Q. Li and T. Wang, *ACS Applied Materials & Interfaces*, 2014, **6**, 15905-15912.
2. C. Feng, J. Zhang, Y. He, C. Zhong, W. Hu, L. Liu and Y. Deng, *ACS Nano*, 2015, **9**, 1730-1739.
3. Q. Liao, N. Li, S. Jin, G. Yang and C. Wang, *ACS Nano*, 2015, **9**, 5310-5317.
4. Y. Haldorai, S. R. Choe, Y. S. Huh and Y.-K. Han, *Carbon*, 2018, **127**, 366-373.
5. D. Xiong, X. Li, Z. Bai, J. Li, H. Shan, L. Fan, C. Long, D. Li and X. Lu, *Electrochimica Acta*, 2018, **259**, 338-347.
6. C. Zhang, J. Xiao, X. L. Lv, L. H. Qian, S. L. Yuan, S. Wang and P. X. Lei, *Journal of Materials Chemistry A*, 2016, **4**, 16516-16523.
7. Y. C. Zheng, Z. Q. Lia, J. Xu, T. L. Wang, X. Liu, X. H. Duan, Y. J. Ma, Y. Zhou and C. H. Pei, *Nano Energy*, 2016, **20**, 94-107.
8. R. Silva, G. M. Pereira, D. Voiry, M. Chhowalla and T. Asefa, *Rsc Adv*, 2015, **5**, 49385-49391.
9. Y. Tinghui, G. Xin, Q. Shengchun, X. Fangyuan, L. Qun, L. Yali, C. Qiang, L. Junshuai and H. Deyan, *Nano-Micro Lett*, 2017, **9**, 38.